Multi-objective optimization of natural convection in a cylindrical annulus mold under magnetic field using particle swarm algorithm ☆

Masoud Afrand [a], Said Farahat [a,*], Alireza Hossein Nezhad [a], Ghanbar Ali Sheikhzadeh [b], Faramarz Sarhaddi [a], Somchai Wongwises [c,*]

[a] Department of Mechanical Engineering, University of Sistan and Baluchestan, Zahedan, Iran
[b] Department of Mechanical Engineering, University of Kashan, Kashan, Iran
[c] Fluid Mechanics, Thermal Engineering and Multiphase Flow Research Lab. (FUTURE), Department of Mechanical Engineering, Faculty of Engineering, King Mongkut's University of Technology Thonburi, Bangmod, Bangkok 10140, Thailand

ARTICLE INFO

ABSTRACT

In the continuous casting process, natural convection occurs in mold containing a liquid metal. Natural convection in the melt causes the impurities to move and this phenomenon can lead to poor product. Therefore, by reducing natural convection, the quality of the product is improved. In this paper, 3D numerical simulation and multi-objective optimization of natural convection in a cylindrical annulus mold filled with molten potassium under a magnetic field is carried out. The inner and outer cylinders are maintained at uniform temperatures and other walls are thermally insulated. Two objective functions including the natural convection heat transfer rate (average Nusselt number) and magnetic field strength have been considered simultaneously. The multi-objective particle swarm optimization algorithm (MOPSO) has been employed. Four decision variables are the Hartmann number, inclination angle, and magnetic field angles. For the optimization process, the calculations of three-dimensional Navier–Stokes, energy, and electrical potential equations are combined with MOPSO. Using the numerically evaluated objective functions, the optimum frontier is estimated by a second order polynomial based on objective functions.

1. Introduction

In the continuous casting process, natural convection occurs in an enclosure filled with a molten metal due to a temperature difference between the solid walls and the molten metal. Natural convection flow in the melt causes the impurities to move. This phenomenon affects the structure of the final product, including ingot, metal slab, and the like. Hence, the melt must have a uniform temperature throughout the enclosure to reduce thermal stresses and natural convection. In recent decades, this problem has been solved by using Magnetohydrodynamics, and natural convection flow has decreased within the enclosures by applying a magnetic field. In the Magnetohydrodynamics, electrically conducting fluid flow in the presence of a magnetic field is investigated. When molten metal (electrically conducting fluid) motion is subjected to a magnetic field, the Lorentz force is generated. It can control growing crystals. This force affects the buoyancy force; thus, the resulting natural convection is suppressed. In these processes, the study and understanding of heat transfer are important, owing to the better control in the

process of producing high-quality products. Consequently, the rate of heat transfer convection should be minimized in this process. Gao et al. [1] proved that imposing a magnetic field leads to products of better quality. They demonstrated that totally equiaxed grains could be obtained in pure aluminum under the external effect of the pulsed magnetic field; yet, only thin columnar grains are formed in high-melting steel, even when treated by the higher magnetic intensity. An analysis of the hydromagnetic natural convection is generally employed in many industrial applications including metal solidification, cooling of electronic equipment, solar technology, heat exchangers, and the like [2–6]. Natural convection in a rectangular cavity has been the subject of a vast number of investigations [7–10]. The annular geometry has been widely investigated by many researchers using experimental, analytical, and numerical methods. Numerically, Afrand et al. [11] studied a steady, laminar, and natural-convection flow under different directions of uniform magnetic field in a long horizontal annulus containing gallium with isothermal walls. Their results revealed that when the strength of a magnetic field is increased, the convection heat transfer is decreased. In another research, they carried out three-dimensional numerical investigations of natural convection in a tilted cylindrical annulus containing molten potassium under various magnetic fields. Their computational results confirmed the effect of the magnetic field direction on natural convection [12]. Wrobel et al. [13] studied convection

Nomenclature

B_0	magnitude of the external magnetic field (kg/s^2A)
D	annulus gap; $D = r_o - r_i(m)$
E	dimensional induced electric field (mkg/s^3A)
E^*	dimensionless induced electric field
F	Lorentz force (N/m^3)
g	acceleration due to gravity (m/s^2)
Ha	Hartmann number
J	electric current density (A/m^2)
L	height of the annulus
Nu	Nusselt number
P	pressure (N/m^2)
Pr	Prandtl number
Ra	Rayleigh number
T	dimensional temperature (K)
T^*	dimensionless temperature
(r, z)	radial and axial co-ordinates
(R, Z)	dimensionless radial and axial co-ordinates
(r_i, r_o)	radii of inner and outer cylinders (m)
(u, v, w)	dimensional velocity components in (r, θ, z) direction (m/s)
(U, V, W)	dimensionless velocity components in (r, θ, z) direction
(x, y, z)	Cartesian c-ordinate components

Greek letters

α	thermal diffusivity (m^2/s)
β	fluid coefficient of thermal expansion $(1/K)$
δ, η	magnetic field angles
φ	dimensional electrical potential (m^2kg/s^3A)
Φ	dimensionless electrical potential
γ	inclination angle
λ	radii ratio
μ	dynamic viscosity (kg/ms)
θ	azimuthal angle
ρ	fluid density (kg/m^3)
σ	fluid electrical conductivity (s^3A^2/m^3kg)

Subscripts

h	condition at hot wall
c	condition at cold wall

Fig. 1. Geometry and coordinates of cavity configuration with magnetic effect.

a low Prandtl number. It was found that the flow and heat transfer were suppressed more effectively by an axial magnetic field in a shallow cavity, whereas in tall cavities, a radial magnetic field was more effective. Furthermore, it was observed that the average Nusselt number increased with the radii ratio but decreased with the Hartmann number. Kakarantzas et al. [17] investigated laminar and turbulent regimes of the liquid metal flow in a vertical annulus under constant horizontal magnetic field numerically. Their results illustrated that when the magnetic field increases, the flow becomes laminar.

Optimization is applied in many fields such as engineering and economic in order to reduce the cost and enhance the quality. In this regard, in recent years, many researches have performed on heat transfer optimization in many different ways [18–20]. In addition, convective heat transfer optimization has been studied by many researchers including Burger et al. [21], Liu et al. [22], Mehrabi et al. [23], Lee and Kim [24], Chen et al. [25], and Jia et al. [26].

By reviewing previous researches, it can be found that most of them have focused on horizontal or vertical cylindrical annulus under constant direction magnetic field. Also, these researches indicated that for an enclosure with constant size and thermo-physical properties, the four parameters including the strength of the magnetic field, the inclination angle of the enclosure, and the spatial angles of the magnetic field are effective on the heat transfer rate [11,12]. It is interesting that despite the attractiveness of optimization problems for engineers, research on multi-objective optimization for convective heat transfer and as the objective functions is not performed. The purpose of this study is to minimize the convective heat transfer by applying a optimized magnetic field in a cylindrical annulus mold containing molten potassium. To achieve this goal, the multi-objective particle swarm optimization algorithm is combined with the SIMPLER algorithm using a FORTRAN computer code.

2. Mathematical formulation

The modeling considered in the present study is an inclined cylindrical annulus formed by two concentric cylinders of inner and outer radii, r_i and r_o, respectively, as shown in Fig. 1. The inner and outer cylinders are maintained at isothermal but different temperatures, T_H and T_C, respectively. The top and bottom walls are assumed to be adiabatic.

in an annular enclosure with a round rod core and a cylindrical outer wall filled with paramagnetic fluid using an experimental and numerical analysis. It is concluded that the magnetic field yielded heat transfer values four times higher than that of the thermal Rayleigh number; thus, it influences heat transfer more efficiently in comparison with increasing the thermal Rayleigh number. Steady, fully developed laminar natural convective flow in open-ended vertical concentric annuli in the presence of a radial magnetic field was considered analytically by Singh and Singh [14]. They corroborated that the Hartmann number and the gap between cylinders play an important role in controlling the behavior of fluid flow. Natural convection in concentric horizontal annuli containing magnetic fluid under non-uniform magnetic fields was investigated experimentally by Sawada et al. [15]. Two concentric cylinders were made of copper and placed horizontally and were maintained at constant temperatures. Various kinds of experiments were performed to clarify the effects of the direction and strength of the magnetic fields on the natural convection. Sankar et al. [16] used an implicit finite difference scheme to simulate the effect of the axial or radial magnetic field on the natural convection in a vertical cylindrical annulus at
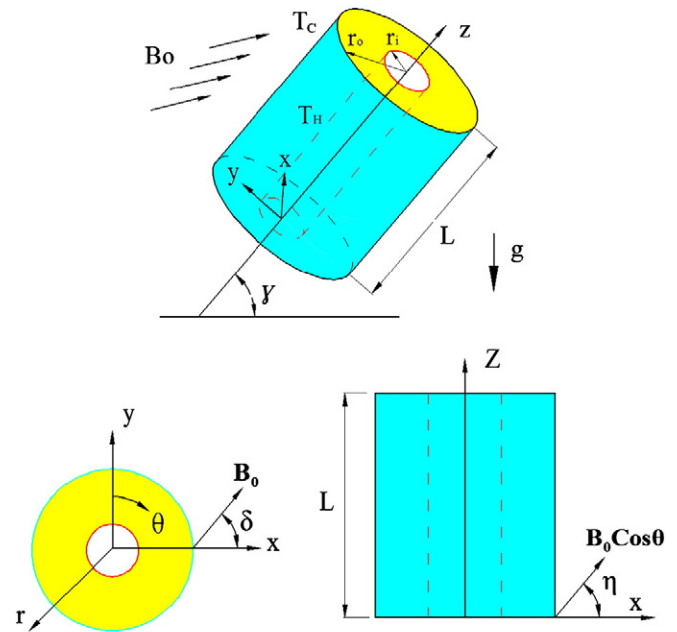
```
┌─────────────────────────────────────────────────────┐
│ For i = 1 to M (M = population size)                  │
│ Initialize P[i] randomly (P is the population of      │
│ particles)                                            │
│ Initialize V [i] = 0 (V = speed of each particle)     │
└─────────────────────────────────────────────────────┘
                        │
                        ▼
┌─────────────────────────────────────────────────────┐
│ Evaluate P[i]                                         │
│ GBEST = Best particle found in P[i]                   │
│ Selecting non-dominated population                    │
│ PBESTS[i]= Best individual position                   │
└─────────────────────────────────────────────────────┘
                        │
                        ▼
┌─────────────────────────────────────────────────────┐
│ Grid spacing and selecting leader                     │◄────┐
└─────────────────────────────────────────────────────┘     │
                        │                                     │
                        ▼                                     │
┌─────────────────────────────────────────────────────┐     │
│ Calculate speed of each particle                      │     │
│ For i = 1 to M                                        │     │
│ V[i] = w × V[i] + C₁ × R₁ × (PBESTS[i] − P[i])        │     │
│ +C₂× R₂ ×(PBESTS[GBEST] − P[i])                       │     │
│ (w = Inertia weight, C1 & C2 are positive constants)  │     │
│ (R₁ & R₂ are random numbers in the range [0..1])      │     │
│ POP[i] = P[i] + V[i]                                  │     │
└─────────────────────────────────────────────────────┘     │
                        │                                     │
                        ▼                                     │
┌─────────────────────────────────────────────────────┐     │
│ Adding non-dominated individual to repository         │     │
└─────────────────────────────────────────────────────┘     │
                        │                                     │
                        ▼                                     │
┌─────────────────────────────────────────────────────┐     │
│ Deleting dominated members of repository              │     │
└─────────────────────────────────────────────────────┘     │
                        │                                     │
                        ▼                                     │
              ╱───────────────────╲         No               │
             ╱ Are convergence     ╲────────────────────────┘
             ╲ criteria satisfied?  ╱
              ╲───────────────────╱
                        │ Yes
                        ▼
                   ( Finish )
```
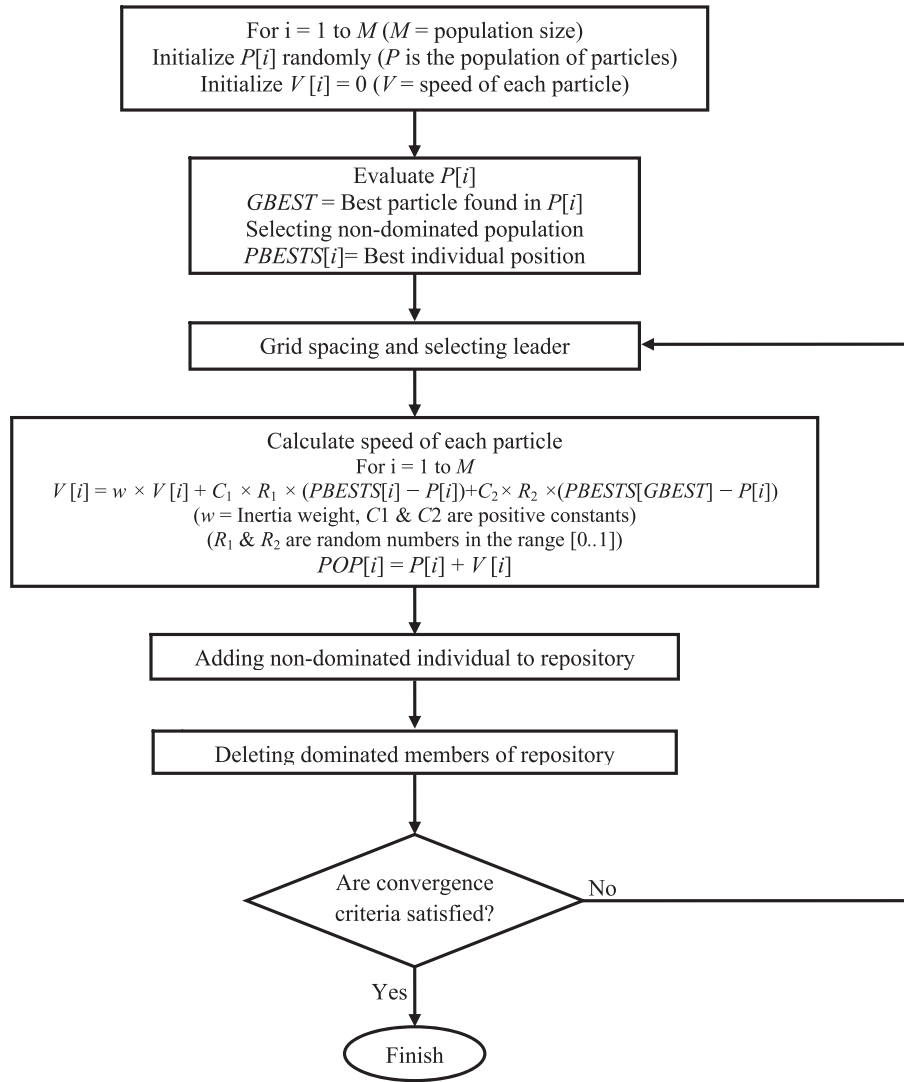
Fig. 2. Multi-objective particle swarm optimization flowchart.

The annulus is filled with molten potassium (Pr = 0.072). The three dimensional cylindrical co-ordinates (r, θ, z) with their corresponding velocity components (u, v, w) are illustrated in Fig. 1. It should be noted that in Fig. 1, g is the gravity acceleration, γ is the inclination angle, and B_0 is a uniform magnetic field. Also, the angles of the magnetic field with different planes are shown in Fig. 1. All walls are assumed to be electrically insulated. In this problem, the angles of the magnetic field and inclination angle must be chosen in such a way that the cost (strength of magnetic field) and rate of heat transfer is minimized.

By using the Boussinesq approximation, the equations governing steady, laminar, Newtonian, and electrically conducting fluid, after neglecting viscous and ohmic dissipations in the three-dimensional cylindrical co-ordinates (r, θ, z), are defined as below:

Continuity equation:

$$\overrightarrow{\nabla}.\overrightarrow{V} = 0 \tag{1}$$

Momentum equation:

$$\left(\overrightarrow{V}.\overrightarrow{\nabla}\right)\overrightarrow{V} = -\frac{1}{\rho}\overrightarrow{\nabla}p + \nu\overrightarrow{\nabla}^2\overrightarrow{V} + \overrightarrow{g} + \overrightarrow{F} \tag{2}$$

Energy equation:

$$\left(\overrightarrow{V}.\overrightarrow{\nabla}\right)T = \alpha\overrightarrow{\nabla}^2 T \tag{3}$$

Electrical potential equation:

$$\overrightarrow{\nabla}^2\varphi = \overrightarrow{\nabla}.\left(\overrightarrow{V} \times \overrightarrow{B}_0\right) = \overrightarrow{V}.\left(\overrightarrow{\nabla} \times \overrightarrow{B}_0\right) + \overrightarrow{B}_0.\left(\overrightarrow{\nabla} \times \overrightarrow{V}\right) \tag{4}$$

Since the magnetic field is constant $(B_0 = cte.)$, the first term of the right side of Eq. (4) is zero.

$$\overrightarrow{J} = \sigma\left(\overrightarrow{E} + \overrightarrow{V} \times \overrightarrow{B}_0\right), \overrightarrow{E} = -\overrightarrow{\nabla}\varphi \text{ and } \overrightarrow{F} = \overrightarrow{J} \times \overrightarrow{B}_0 \tag{5}$$

Table 1
Grid independence test.

Grid	$21 \times 61 \times 31$	$41 \times 61 \times 61$	$81 \times 61 \times 121$
Nu	4.923	5.245	5.321
Error	6.1%	1.4%	–

$\vec{V}$ is the vector of velocity, p is the pressure, μ is the dynamic viscosity, ρ is the fluid density, T is the temperature, α is the thermal diffusivity, β is the coefficient of volumetric expansion, σ is the electrical conductivity, $\vec{E}$ is the induced electrical field vector, $\vec{J}$ is the electric current density vector, $\vec{F}$ is the Lorentz force vector, and φ is the electrical potential.

Besides, ∇ and ∇^2 are the gradient and Laplacian operators, respectively.

For convenience, the governing equations are nondimensionalized using the following parameters:

$$U = \frac{uD}{\alpha}, V = \frac{vD}{\alpha}, W = \frac{wD}{\alpha}, R = \frac{r}{D}, Z = \frac{z}{L}, A = \frac{L}{D},$$
$$P = \frac{pD^2}{\rho\alpha^2}, T^* = \frac{T-T_c}{T_h-T_c}, \Phi = \frac{\varphi}{B_0\alpha}, E^* = \frac{ED}{B_0\alpha} \tag{6}$$

In Eq. (6), D and L are the height and gap of annulus, respectively.

With some mathematical manipulations, the governing equations given by Eqs. (1)–(4) can be expressed in a dimensionless form as:

a)

b)

Fig. 3. Comparison of average Nusselt number results with data in the literature. (a) Experimental data and (b) numerical data.

Dimensionless continuity equation:

$$\frac{\partial U}{\partial R} + \frac{1}{R}\frac{\partial V}{\partial \theta} + \frac{1}{A}\frac{\partial W}{\partial Z} = 0 \tag{7}$$

Dimensionless momentum equation: r component:

$$U\frac{\partial U}{\partial R} + \frac{V}{R}\frac{\partial U}{\partial \theta} - \frac{V^2}{R} + \frac{1}{A}W\frac{\partial U}{\partial Z} = -\frac{\partial P}{\partial R}$$
$$+ \Pr\left[\frac{\partial^2 U}{\partial R^2} + \frac{1}{R}\frac{\partial U}{\partial R} + \frac{1}{R^2}\frac{\partial^2 U}{\partial \theta^2} + \frac{1}{A^2}\frac{\partial^2 U}{\partial Z^2} - \frac{U}{R^2} - \frac{2}{R^2}\frac{\partial V}{\partial \theta}\right] + Ra.\Pr.T^* Cos\gamma Cos\theta$$
$$+ Ha^2.\Pr\left(\frac{1}{R}\frac{\partial \Phi}{\partial \theta}(Cos\delta Sin\eta) - \frac{1}{A}\frac{\partial \Phi}{\partial Z}(Cos\delta Cos\eta Cos\theta - Sin\delta Sin\theta)\right)$$
$$- Ha^2.\Pr U\left(Cos^2\delta Cos^2\eta Cos^2\theta - \frac{1}{2}Sin2\delta Cos\eta Sin2\theta + Sin^2\delta Sin^2\theta\right)$$
$$+ \frac{Ha^2.\Pr.V}{2}\left[Sin2\theta\left(Cos^2\delta Cos^2\eta - Sin^2\delta\right) + Sin2\delta Cos\eta Cos2\theta\right]$$
$$- Ha^2.\Pr\left[U\left(Cos^2\delta Sin^2\eta\right) - \frac{W}{2}\left(Cos^2\delta Sin2\eta Sin\theta + Sin2\delta Sin\eta Cos\theta\right)\right] \tag{8}$$

θ component:

$$U\frac{\partial V}{\partial R} + \frac{V}{R}\frac{\partial V}{\partial \theta} + \frac{UV}{R} + \frac{1}{A}W\frac{\partial V}{\partial Z} = -\frac{1}{R}\frac{\partial P}{\partial \theta}$$
$$+ \Pr\left[\frac{\partial^2 V}{\partial R^2} + \frac{1}{R^2}\frac{\partial^2 V}{\partial \theta^2} + \frac{1}{R}\frac{\partial V}{\partial R} + \frac{1}{A^2}\frac{\partial^2 V}{\partial Z^2} - \frac{V}{R^2} + \frac{2}{R^2}\frac{\partial U}{\partial \theta}\right] - Ra.\Pr.T^* Cos\gamma Sin\theta$$
$$+ Ha^2.\Pr\left(\frac{1}{A}\frac{\partial \Phi}{\partial Z}(Cos\delta Cos\eta Sin\theta + Sin\delta Cos\theta) - \frac{\partial \Phi}{\partial R}(Cos\delta Sin\eta)\right)$$
$$- Ha^2.\Pr\left[V\left(Cos^2\delta Sin^2\eta\right) + W\left(Cos^2\delta Cos2\eta Cos\theta - \frac{1}{2}Sin2\delta Sin\eta Sin\theta\right)\right]$$
$$+ \frac{Ha^2.\Pr.U}{2}\left[Sin2\theta\left(Cos^2\delta Cos^2\eta - Sin^2\delta\right) + Sin2\delta Cos\eta Cos2\theta\right]$$
$$- Ha^2.\Pr.V\left(Cos^2\delta Cos^2\eta Sin^2\theta + \frac{1}{2}Sin2\delta Cos\eta Sin2\theta + Sin^2\delta Cos^2\theta\right) \tag{9}$$

z component:

$$U\frac{\partial W}{\partial R} + \frac{V}{R}\frac{\partial W}{\partial \theta} + \frac{1}{A}W\frac{\partial W}{\partial Z} = -\frac{1}{A}\frac{\partial P}{\partial Z}$$
$$+ \Pr\left[\frac{\partial^2 W}{\partial R^2} + \frac{1}{R^2}\frac{\partial^2 W}{\partial \theta^2} + \frac{1}{R}\frac{\partial W}{\partial R} + \frac{1}{A^2}\frac{\partial^2 W}{\partial Z^2}\right] + Ra.\Pr.T^* Sin\gamma$$
$$+ Ha^2.\Pr\frac{\partial \Phi}{\partial R}(Cos\delta Cos\eta Cos\theta - Sin\delta Sin\theta)$$
$$- Ha^2.\Pr\frac{1}{R}\frac{\partial \Phi}{\partial \theta}(Cos\delta Cos\eta Sin\theta + Sin\delta Cos\theta)$$
$$+ \frac{Ha^2.\Pr.U}{2}\left(Cos^2\delta Sin2\eta Sin\theta + Sin2\delta Sin\eta Cos\theta\right)$$
$$- Ha^2.\Pr.W\left(Cos^2\delta Cos^2\eta Sin^2\theta + \frac{1}{2}Sin2\delta Cos\eta Sin2\theta + Sin^2\delta Cos^2\theta\right)$$
$$+ \frac{Ha^2.\Pr.V}{2}\left(Cos^2\delta Sin2\eta Cos\theta - Sin2\delta Sin\eta Sin\theta\right)$$
$$- Ha^2.\Pr.W\left(Cos^2\delta Cos^2\eta Cos^2\theta - \frac{1}{2}Sin2\delta Cos\eta Sin2\theta + Sin^2\delta Sin^2\theta\right) \tag{10}$$

Dimensionless energy equation:

$$U\frac{\partial T^*}{\partial R} + \frac{V}{R}\frac{\partial T^*}{\partial \theta} + \frac{1}{A}W\frac{\partial T^*}{\partial Z} = \frac{\partial^2 T^*}{\partial R^2} + \frac{1}{R^2}\frac{\partial^2 T^*}{\partial \theta^2} + \frac{1}{R}\frac{\partial T^*}{\partial R} + \frac{1}{A^2}\frac{\partial^2 T^*}{\partial Z^2} \tag{11}$$
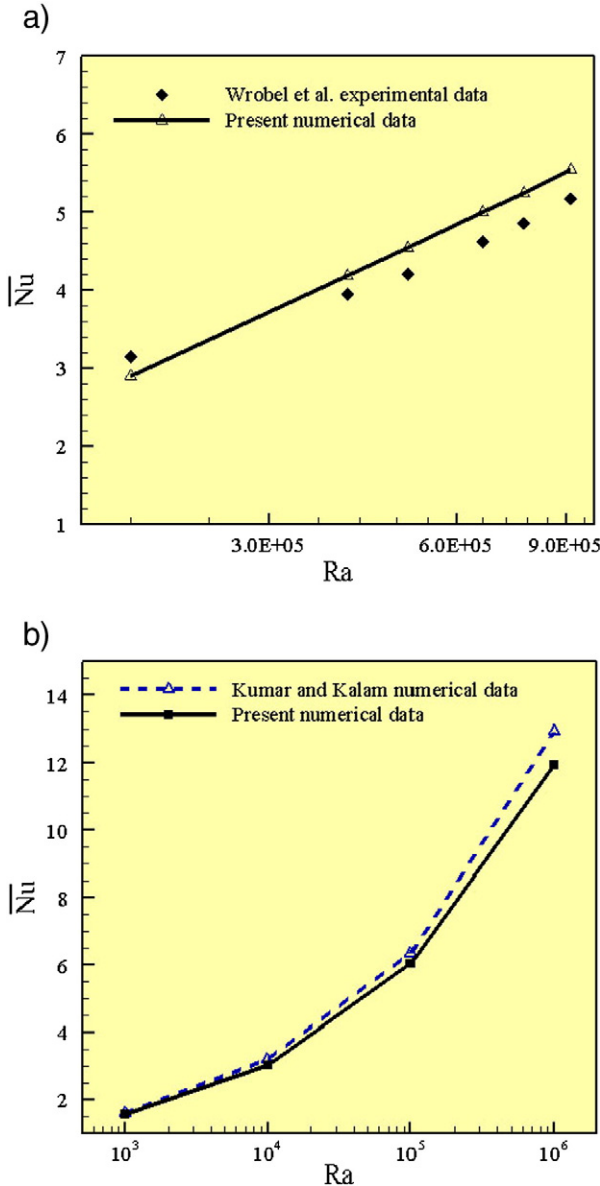
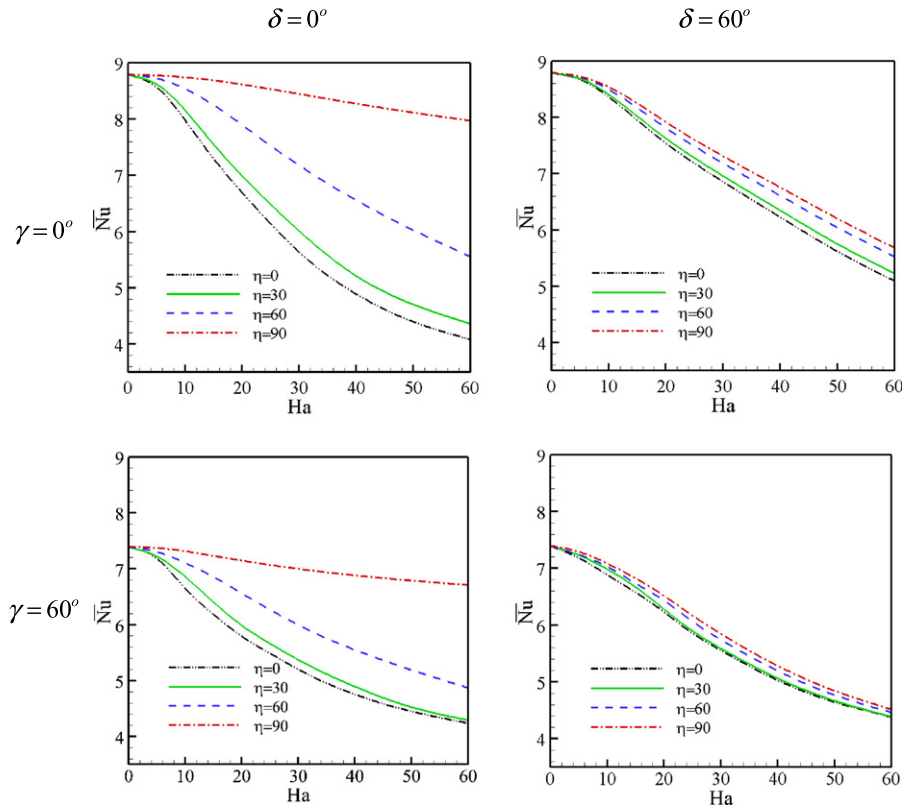$$\delta = 0^o \qquad\qquad\qquad \delta = 60^o$$

Fig. 4. The average Nusselt number versus Hartmann number for different inclination angle and angles of magnetic field.

Dimensionless electrical potential equation:

$$\frac{\partial^2 \Phi}{\partial R^2} + \frac{1}{R^2}\frac{\partial^2 \Phi}{\partial \theta^2} + \frac{1}{R}\frac{\partial \Phi}{\partial R} + \frac{\partial^2 \Phi}{\partial Z^2} =$$

$$(Cos\delta\, Cos\eta\, Sin\theta + Sin\delta\, Cos\theta)\left(\frac{1}{R}\frac{\partial W}{\partial \theta} - \frac{1}{A}\frac{\partial V}{\partial Z}\right)$$

$$+(Cos\delta\, Cos\eta\, Cos\theta - Sin\delta\, Sin\theta)\left(\frac{1}{A}\frac{\partial U}{\partial Z} - \frac{\partial W}{\partial R}\right)$$

$$+(Cos\delta\, Sin\eta)\left(\frac{V}{R} + \frac{\partial V}{\partial R} - \frac{1}{R}\frac{\partial U}{\partial \theta}\right) \qquad (12)$$

In the above equations, Pr is the Prandtl number and *Ra* is the Rayleigh number defined as follows:

$$Pr = \frac{\upsilon}{\alpha}, \ Ra = \frac{g\beta(T_H - T_C)D^3}{\upsilon\alpha} \qquad (13)$$

The effect of the magnetic field is introduced into the momentum and potential equations through the Hartmann number. The Hartmann number is defined as:

$$Ha = B_0 D\sqrt{\frac{\sigma}{\mu}} \qquad (14)$$

The local and average Nusselt numbers along the inner cylinder are defined as follows:

$$Nu(\theta,Z) = \frac{\partial T^*}{\partial R}\Big|_{R=R_i}, \ \overline{Nu} = \frac{1}{2\pi L}\int_0^{2\pi}\int_0^L Nu(\theta,Z)\,dZd\theta \qquad (15)$$

No-slip conditions are assumed on all walls. Constant temperatures at the inner ($T_i^* = 1$) and outer ($T_o^* = 0$) cylindrical walls, and adiabatic conditions are considered at the bottom and top walls ($\partial T^*/\partial Z = 0$). In addition, all walls are assumed to be electrically insulated ($\partial\Phi/\partial n = 0$).

3. Method of solution

In this paper, a FORTRAN computer code is applied. Due to the various parameters and time consuming calculations, to lower the numbers of calculations, the MOPSO algorithm is combined with the SIMPLER algorithm. Hence, selecting the angles (γ, δ and η) and strength of the magnetic field (*Ha*) leads to the optimal solution and extra computation is avoided.

In order to solve the governing equations, a numerical method based on the finite volume is used. The diffusion terms in the governing equations are discretized using a second-order central difference scheme. Meanwhile, this method is used to discretize the convection terms for the hybrid-scheme, which is a combination of the central difference scheme and the upwind scheme. A staggered grid system along with the SIMPLER algorithm is adopted to solve the governing equations. The coupled systems of discretized equations are solved iteratively using the TDMA method [27]. To obtain the converged solutions, an under-relaxation scheme is employed.

For multi-objective optimization, several methods are developed, which are explained in various references [28]. As the speed of convergence in the particle swarm algorithm is more than the genetic algorithm, this algorithm, which is based on the initial population introduced firstly by Kennedy and Eberhart [29], is applied to perform optimization. Objective functions constraint and decision

variables are important points. In this problem, Ha is regarded as both a decision variable and cost function. The multi-objective optimization problem is defined as follows:

$$\begin{cases} \text{Minimize}: \ \overline{Nu} = f_1(\gamma, \delta, \eta, Ha), \ \ Ha \\ \text{subjected to} \\ 0^o \leq \gamma \leq 90^o \\ 0^o \leq \delta \leq 90^o \\ 0^o \leq \eta \leq 90^o \\ 0 \leq Ha \leq 60 \end{cases} \quad (16)$$

At first, 40 sets of $[\gamma, \delta, \eta, Ha]$ are produced randomly in the specified range, then the objective function including $\overline{Nu}$ and Ha is calculated. In the next step, the non-dominated members defined by Eq. (17) are saved. In this way, the best position in the population (gbest) is obtained.

$$(\gamma, \delta, \eta, Ha)_p \ dominate \ (\gamma, \delta, \eta, Ha)_q \Longleftrightarrow \begin{cases} \forall : \ (\overline{Nu} \ \& \ Ha)_p \leq (\overline{Nu} \ \& \ Ha)_q \\ and \\ \exists : \ (\overline{Nu} \ or \ Ha)_p < (\overline{Nu} \ or \ Ha)_q \end{cases} \quad (17)$$

Afterward, the velocity of each particle in the ith iteration is calculated as follows:

$$\begin{aligned} v_\gamma^i &= \omega v_\gamma^{i-1} + C_1 r_1 \left[p_{best,i} - \gamma^{i-1} \right] + C_2 r_2 \left[g_{best} - \gamma^{i-1} \right] \\ v_\delta^i &= \omega v_\delta^{i-1} + C_1 r_1 \left[p_{best,i} - \delta^{i-1} \right] + C_2 r_2 \left[g_{best} - \delta^{i-1} \right] \\ v_\eta^i &= \omega v_\eta^{i-1} + C_1 r_1 \left[p_{best,i} - \eta^{i-1} \right] + C_2 r_2 \left[g_{best} - \eta^{i-1} \right] \\ v_{Ha}^i &= \omega v_{Ha}^{i-1} + C_1 r_1 \left[p_{best,i} - (Ha)^{i-1} \right] + C_2 r_2 \left[g_{best} - (Ha)^{i-1} \right] \end{aligned} \quad (18)$$

The new position of the particle is acquired by Eq. (19), and the objective function for each particle is calculated. The mentioned steps are repeated until the convergence criterion is satisfied. The MOPSO algorithm is illustrated in Fig. 2.

$$\begin{aligned} \gamma^i &= \gamma^{i-1} + v_\gamma^i \\ \delta^i &= \delta^{i-1} + v_\delta^i \\ \eta^i &= \eta^{i-1} + v_\eta^i \\ (Ha)^i &= (Ha)^{i-1} + v_{Ha}^i \end{aligned} \quad (19)$$

4. Grid study and validation

The different grid sizes are examined to ensure grid independence results. The tested grids and the obtained average Nusselt numbers are demonstrated in Table 1. The results are obtained for inclined annulus with $\lambda = 6.0$, $A = 3.0$, and $\gamma = 45^o$, and containing molten potassium with Pr = 0.072. The Hartmann and Rayleigh numbers are 30 and 10^5, respectively. According to Table 1, a $41 \times 61 \times 61$ grid is sufficiently fine in r, θ, and z directions, respectively.

In order to approve the numerical procedure, two test cases are examined using the proposed code. In the first test, the results are compared with the existing experimental results in the literature. In the absence of a magnetic field, the numerical results are firstly validated with Wrobel et al. [13]. Experimental data is illustrated in Fig. 3(a). The maximum discrepancy is within 8%. In the second test, a

comparison is made between the present results and Kumar and Kalam [30]. Numerical data is depicted in Fig. 3(b). It can be seen that there is an agreement between the results.
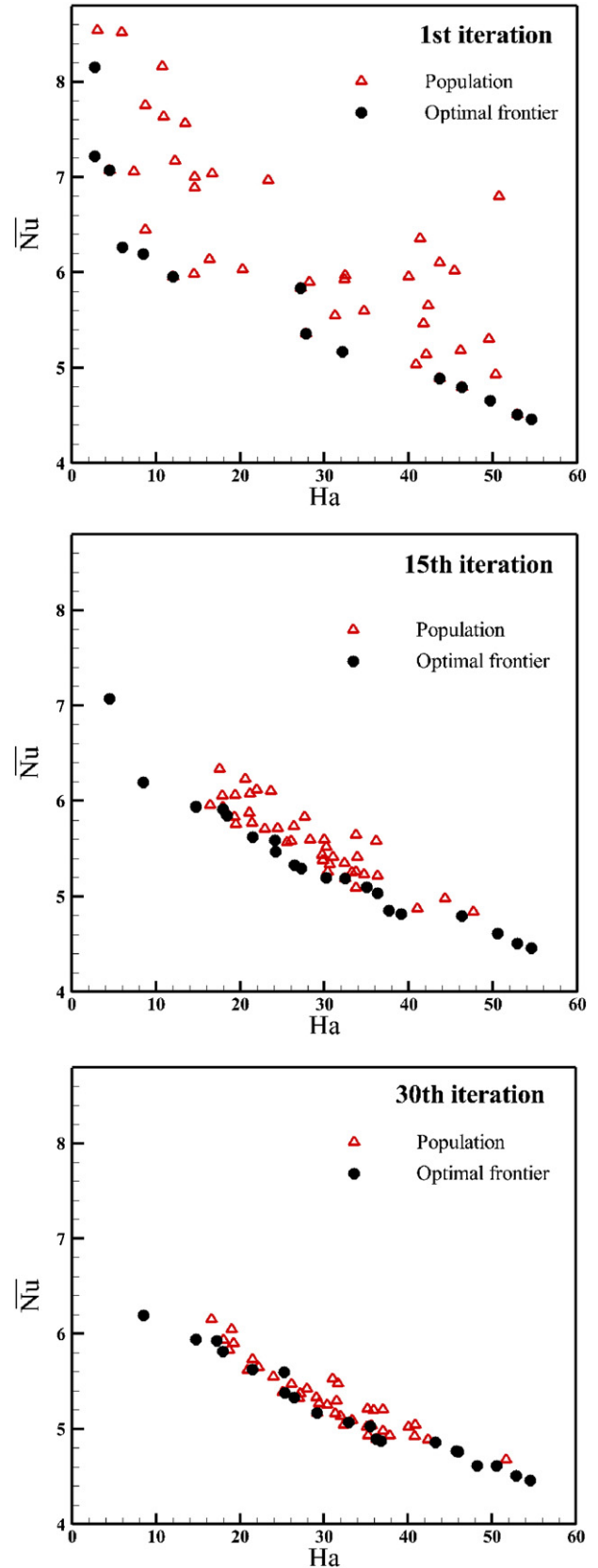

Fig. 5. Population and optimal frontier in different iterations.

Table 2
Optimal frontier values and decision variables related to each of them.

γ	δ	η	Ha	$\overline{Nu}$
85.29	14.62	27.99	8.46	6.19
54.13	81.83	52.65	54.55	4.46
34.62	13.69	27.44	52.90	4.51
58.34	81.55	28.22	50.51	4.61
83.47	71.27	27.12	14.76	5.94
81.40	41.15	33.90	21.47	5.62
84.90	46.21	27.44	26.47	5.33
82.38	26.59	33.64	17.21	5.92
51.94	38.42	50.86	45.71	4.77
81.39	35.91	25.59	17.91	5.81
58.99	36.46	46.43	45.99	4.76
64.65	49.64	35.99	43.29	4.86
80.46	50.52	27.56	25.30	5.38
73.65	47.69	33.50	48.24	4.61
83.94	55.50	30.41	32.95	5.07
83.68	49.67	33.29	36.76	4.87
69.46	43.93	28.42	25.20	5.59
78.88	47.69	32.36	36.24	4.90
84.00	48.32	29.58	29.12	5.17
86.53	53.98	26.85	35.46	5.03

5. Results and discussion

The natural convection of a low Prandtl number electrically conducting fluid in an inclined cylindrical annulus mold with isothermally heated and cooled vertical walls, and adiabatic top and bottom walls in the presence of a uniform magnetic field, is studied numerically. In the present study, the aspect ratio of A = 3 and radii ratio of $\lambda = 6$ are selected [17]. Simulations are performed for a wide range of the Hartmann number ($0 \leq Ha \leq 60$), inclination angle ($0^o \leq \gamma \leq 90^o$), and angles of the magnetic field ($0^o \leq \delta \leq 90^o$ and $0^o \leq \eta \leq 90^o$). Furthermore, it is assumed that $Ra = 10^5$ and $Pr = 0.072$. Then, multi-objective optimization of the natural convection in the mold using the particle swarm algorithm is performed.

Fig. 4 shows the average Nusselt number versus the Hartmann number for different inclination angles and angles of the magnetic field. Comparing different cases illustrated an increase in Ha and a reduction in $\overline{Nu}$ caused by γ. In addition, for specified γ and η by increasing δ, the effect of Ha on $\overline{Nu}$ decreases. For specified Ha and γ by increasing δ, the effect of η on $\overline{Nu}$ decreases. It can be seen from this figure that for the specified Ha, γ, and δ, when $\eta \leq 30^o$ and the effect of η on $\overline{Nu}$ is negligible but for $\eta > 30^o$, this effect is significant. It can be found from Fig. 4 and Eq. (5) that the Lorentz force depends on two factors: the induced

Fig. 6. Optimal frontier in objectives' space $\left(\overline{Nu} - Ha\right)$ and fitted curve.

electric field and $\left(\vec{V} \times \vec{B_0}\right)$. Therefore, it can be concluded that the interaction of these parameters is in a way that the induced electric field decreases the Lorentz force and $\left(\vec{V} \times \vec{B_0}\right)$ increases the Lorentz force in the present annulus. Since the Lorentz force plays an important role in the reduction of natural convection, the direction of the magnetic field is effective on the average Nusselt number. (See Fig. 4.)

Fig. 4 clearly showed the complexity of the relationship between the parameters. This figure demonstrated the importance of optimization in this problem. Because optimization makes the review all cases averted.

The optimization is performed by MOPSO using four parameters (γ, δ, η, Ha). All results are obtained considering $Ra = 10^5$, $Pr = 0.072$, $\lambda = 6$, and $A = 3$. Fig. 5 shows how the particles get closer to the optimal frontier in different iterations. It can be observed that after 15 iterations, results do not show immense changes. The optimal frontier values and decision variables related to each of them are shown in Table 2. In Fig. 6, the plot of the optimal frontier for objective functions is presented. It can be seen in Fig. 6 that by increasing the Hartmann number, the average Nusselt number decreases. To assist the optimal selection of the magnetic field direction, the Hartmann number, inclination angle, and fitted curve ($\overline{Nu} = 4.12 \times 10^{-4}Ha^2 - 6.47 \times 10^{-2}Ha + 6.80$), which is valid in the range of $8.46 \leq Ha \leq 54.55$, are derived for the optimal points curve.

6. Conclusion

The natural convection of molten potassium in an inclined cylindrical annulus with isothermally heated and cooled vertical walls, and adiabatic top and bottom walls in the presence of a uniform magnetic field, is studied numerically. Simulations are performed for a wide range of the Hartmann number, inclination angle, and magnetic field direction. Results indicated the complexity of the relationship between the parameters. To get rid of this complexity and reduce the computational complexity, the MOPSO algorithm is combined with the SIMPLER algorithm. The optimization is performed by MOPSO regarding the Hartmann number, inclination angle, and magnetic field angles. The average Nusselt and Hartmann numbers were considered simultaneously for multi-objective optimization. The optimal frontier in the objectives space was obtained. To assist the optimal selection of the magnetic field direction, the Hartmann number, inclination angle, and fitted curve $\left(\overline{Nu} = 4.12 \times 10^{-4}Ha^2 - 6.47 \times 10^{-2}Ha + 6.80\right)$, which is valid in the range of $8.46 \leq Ha \leq 54.55$, are derived for the optimal points curve.

References

[1] Y.L. Gao, Q.S. Li, Y.Y. Gong, Q.J. Zhai, Comparative study on structural transformation of low-melting pure Al and high-melting stainless steel under external pulsed magnetic field, Mater. Lett. 61 (2007) 4011–4014.
[2] Y. Okano, S. Sakai, H. Yamada, K. Hoshikawa, S. Dost, Marangoni convection in a hemispheric molten silicon droplet and its control by an applied magnetic field, Int. J. Appl. Electromagn. Mech. 18 (2003) 187–197.
[3] J. Pal, A. Cramer, G. Gerbeth, Experimental investigation on the electromagnetically controlled buoyancy-induced flow in a model of a Czochralski puller, Int. J. Appl. Electromagn. Mech. 44 (2014) 163–170.
[4] G.H.R. Kefayati, Simulation of magnetic field effect on natural convection of non-Newtonian power-law fluids in a sinusoidal heated cavity using FDLBM, Int. Commun. Heat Mass Transf. 53 (2014) 139–153.
[5] T.P. Bednarz, C. Lei, J.C. Patterson, H. Ozoe, Suppressing Rayleigh–Benard convection in a cube using a strong magnetic field—experimental heat transfer rate measurements and flow visualization, Int. Commun. Heat Mass Transf. 36 (2009) 97–102.
[6] C. Maatki, L. Kolsi, H.F. Oztop, A. Chamkha, M. Naceur Borjini, H.B. Aissia, K. Al-Salem, Effects of magnetic field on 3D double diffusive convection in a cubic cavity filled with a binary mixture, Int. Commun. Heat Mass Transf. 49 (2013) 86–95.
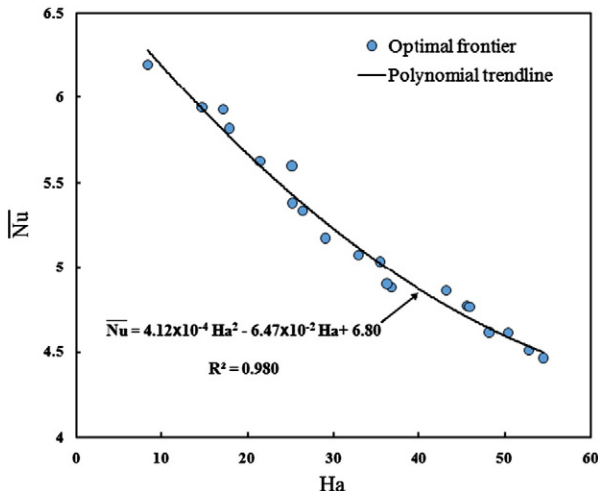
[7] N. Rudraiah, R.M. Barron, M. Venkatachalappa, C.K. Subbaraya, Effect of a magnetic field on free convection in a rectangular enclosure, Int. J. Eng. Sci. 33 (1995) 1075–1084.

[8] P.X. Yu, J.X. Qiu, Q. Qin, Z.F. Tian, Numerical investigation of natural convection in a rectangular cavity under different directions of uniform magnetic field, Int. J. Heat Mass Transfer 67 (2013) 1131–1144.

[9] G.A. Sheikhzadeh, A. Fattahi, M.A. Mehrabian, Numerical study of steady magneto-convection around an adiabatic body inside a square enclosure in low Prandtl numbers, Heat Mass Transf. 47 (2011) 27–34.

[10] M. Pirmohammadi, M. Ghassemi, Effect of magnetic field on convection heat transfer inside a tilted square enclosure, Int. Commun. Heat Mass Transf. 36 (2009) 776–780.

[11] M. Afrand, S. Farahat, A. Hossein Nezhad, G.A. Sheikhzadeh, F. Sarhaddi, Numerical simulation of electrically conducting fluid flow and free convective heat transfer in an annulus on applying a magnetic field, Heat Trans Res 45 (2014) 749–766.

[12] M. Afrand, S. Farahat, A. Hossein Nezhad, G.A. Sheikhzadeh, F. Sarhaddi, 3-D numerical investigation of natural convection in a tilted cylindrical annulus containing molten potassium and controlling it using various magnetic fields, Int J App Electromagn Mech 46 (2014) 809–821.

[13] W. Wrobel, E. Fornalik-Wajs, J.S. Szmyd, Experimental and numerical analysis of thermo-magnetic convection in a vertical annular enclosure, Int. J. Heat Fluid Flow 31 (2010) 1019–1031.

[14] R.K. Singh, A.K. Singh, Effect of induced magnetic field on natural convection in vertical concentric annuli, Acta Mech. Sin. 28 (2012) 315–323.

[15] T. Sawada, H. Kikura, A. Saito, T. Tanahashi, Natural convection of a magnetic fluid in concentric horizontal annuli under nonuniform magnetic fields, Exp. Thermal Fluid Sci. 7 (1993) 212–220.

[16] M. Sankar, M. Venkatachalappa, I.S. Shivakumara, Effect of magnetic field on natural convection in a vertical cylindrical annulus, Int. J. Eng. Sci. 44 (2006) 1556–1570.

[17] S.C. Kakarantzas, I.E. Sarris, N.S. Vlachos, Natural convection of liquid metal in a vertical annulus with lateral and volumetric heating in the presence of a horizontal magnetic field, Int. J. Heat Mass Transfer 54 (2011) 3347–3356.

[18] L. Gosselin, M. Tye-Gingras, F. Mathieu-Potvin, Review of utilization of genetic algorithms in heat transfer problems, Int. J. Heat Mass Transfer 52 (2009) 2169–2188.

[19] W. Liu, Z.C. Liu, H. Jia, A.W. Fan, A. Nakayama, Entransy expression of the second law of thermodynamics and its application to optimization in heat transfer process, Int. J. Heat Mass Transfer 54 (2011) 3049–3059.

[20] N. Amanifard, N. Nariman-Zadeh, M. Borji, A. Khalkhali, A. Habibdoust, Modelling and Pareto optimization of heat transfer and flow coefficients in microchannels using GMDH type neural networks and genetic algorithms, Energy Convers. Manag. 49 (2008) 311–325.

[21] F.H. Burger, J. Dirker, J.P. Meyer, Three-dimensional conductive heat transfer topology optimisation in a cubic domain for the volume-to-surface problem, Int. J. Heat Mass Transfer 67 (2013) 214–224.

[22] W. Liu, H. Jia, Z.C. Liu, H.S. Fang, K. Yang, The approach of minimum heat consumption and its applications in convective heat transfer optimization, Int. J. Heat Mass Transfer 57 (2013) 389–396.

[23] M. Mehrabi, M. Sharifpur, J.P. Meyer, Modelling and multi-objective optimisation of the convective heat transfer characteristics and pressure drop of low concentration TiO$_2$–water nanofluids in the turbulent flow regime, Int. J. Heat Mass Transfer 67 (2013) 646–653.

[24] Ki-Don Lee, Kwang-Yong Kim, Objective function proposed for optimization of convective heat transfer devices, Int. J. Heat Mass Transfer 55 (2012) 2792–2799.

[25] Q. Chen, M. Wang, N. Pan, Z.Y. Guo, Optimization principles for convective heat transfer, Energy 34 (2009) 1199–1206.

[26] H. Jia, Z.C. Li, W. Liu, A. Nakayama, Convective heat transfer optimization based on minimum entransy dissipation in the circular tube, Int. J. Heat Mass Transfer 73 (2014) 124–129.

[27] S.V. Patankar, Numerical Heat Transfer and Fluid Flow, Hemisphere, 1980. (New York).

[28] C.A. Coello Coello, G.B. Lamont, D.A. Van Veldhuizen, Evolutionary Algorithms for Solving Multi-Objective Problems, 2nd edition Springer, 2007.

[29] J. Kennedy, R.C. Eberhart, Particle Swarm Optimization, Proc. IEEE Int. Conf. Neural Networks, Piscataway, New Jersey, 1995, pp. 1942–1948.

[30] R. Kumar, M.A. Kalam, Laminar thermal convection between vertical coaxial isothermal cylinders, Int. J. Heat Mass Transfer 34 (1991) 513–524.